Dyes and Pigments 221 (2024) 111760

Contents lists available at ScienceDirect

Dyes and Pigments

journal homepage: www.elsevier.com/locate/dyepig

Mechanochromism, tunable pure organic room temperature phosphorescence, single-molecule near-white emission, digital encryption, and anti-counterfeiting

Jianmei Guo [a,1], Chenwei Hu [b,1], Jiaqi Liu [b], Yongtao Wang [a,*], Lei Ma [b,**]

[a] Guangxi Key Laboratory of Electrochemical and Magneto-chemical Function Materia, College of Chemistry and Bioengineering, Guilin University of Technology, Guilin, 541004, China

[b] Tianjin International Center for Nanoparticles and Nanosystem, Tianjin University, Tianjin, 300072, China

ARTICLE INFO

Keywords:
Room-temperature phosphorescence
Single-molecule white-light emission
Mechanochromism
Anti-counterfeiting
Imidazopyridine derivatives

ABSTRACT

The development of tunable pure organic room temperature phosphorescence and single-molecule white light emitters still faces a great challenge due to ineffective intersystem crossing and sensitive triplet excitons. Here, two phenothiazine based luminogens named PtzIP and PtzIPCN were designed and synthesized. PtzIP exhibits mechanochromic activity with hypsochromic shift of 25 nm, tunable room temperature phosphorescence from 613 nm to 530 nm and 560 nm, then to 540 nm and 585 nm by crushing and grinding, and single-molecule near-white light emission with the (CIE: Commission International de l'Eclairage) CIE coordinates of (0.33, 0.25), but PtzIPCN shows mechanochromism and room temperature phosphorescence inertness in crystalline state. By choosing polymethyl methacrylate (PMMA) and 4-fluorobenzophenone(F-BP) as host materials, as well PtzIP and PtzIPCN as guest materials, a series of host-guest doping systems were constructed and optimized by tuning doping ratio. PtzIP/PMMA and PtzIPCN/PMMA doping systems present concentration dependent fluorescence and phosphorescence emission, and RTP lifetime and afterglow of PtzIPCN/PMMA are up to 185.31 ms of 2.0 s. Furthermore, the lifetime of F-BP/PtzIPCN increases to 216.63 ms at doping ratio of 1:1000 for F-BP and PtzIPCN. Based on different luminescent properties of PtzIP and PtzIPCN in the doping systems, a series of high-level digital encryption and anti-counterfeiting patterns were successfully constructed. More importantly, the underlying mechanism behind luminescent properties were explored in detail by photophysical testing, crystal analysis, and theoretical calculations.

1. Introduction

Pure organic room temperature phosphorescence (*p*-RTP) materials have broad application prospects in high-tech fields such as information storage and anti-counterfeiting encryption, bioimaging, and optical sensing [1–4]. Theoretically, incorporating heteroatoms (N, O, S and P) and carbonyl can boost the spin-orbital coupling (SOC) between excited singlet (S_1) and triplet states (T_1), and thereby promote intersystem crossing (ISC) [5–11]. By designing D (electron donor)-A (electron acceptor) and D-π-A type luminogens, the energy gap between S_1 and T_1 (ΔE_{ST}) can be effectively tuned to inhibit the reverse ISC process [12–14]. In addition, constructing rigid environment such as intermolecular hydrogen bonds, host-guest doping, crystal engineering, and H aggregation can suppress the non-radiative decay of triplet excitons, facilitating discovery of room temperature phosphorescence (RTP) materials with high efficiency and long lifetime [15–21]. Following the above-mentioned principles, more and more *p*-RTP materials are constantly discovered, and excellent performance is continuously refreshed. Even so, stimuli-responsive *p*-RTP materials with phosphorescence wavelength shift and single-molecule white light emitters (SMWLE) composed of fluorescence and phosphorescence are rarely reported.

Under the stimulation of external forces such as grinding, scraping, and crushing, fluorescence materials with mechanochromic activity show significant changes in fluorescence signals due to phase transition from crystalline to amorphous states/crystalline, or from amorphous

* Corresponding author.
** Corresponding author.
E-mail addresses: wyt_shzu@163.com (Y. Wang), lei.ma@tju.edu.cn (L. Ma).
[1] Jianmei Guo and Chenwei Hu contributed equally.

https://doi.org/10.1016/j.dyepig.2023.111760
Received 29 August 2023; Received in revised form 7 October 2023; Accepted 12 October 2023
Available online 26 October 2023

states to crystalline. But for phosphorescent materials, mechanical force often leads to the quenching of RTP due to the sensitivity of triplet excitons to oxygen and vibration [22], which also makes tunable phosphorescence materials with wavelength shift scarce despite being more desirable and profitable. Furthermore, crystalline small molecules and host-guest doping systems make up the majority of *p*-RTP materials [23,24]. Among of them, some exhibit different phosphorescence emission in crystalline and host-guest doping systems, and even show doping concentration-dependent RTP emission in doping systems, while others maintain a constant phosphorescence wavelength in crystalline and different doping matrix, but the underlying mechanism is difficult to elucidate [25–28]. What is worse, it is difficult to clarify molecular configuration, and intermolecular interactions and stacking modes of phosphorescent chromophores in polymer and amorphous states [29]. As a result, the mechanism behind phosphorescence changes in crystalline states and different doped matrices is still vague, which also leads to lack of molecular design rules of tunable phosphorescent luminogens.

Owing to the increased need in display applications and advanced lighting, organic white-light devices are gaining more and more attention. White-light devices are often fabricated by combining three primary or two complementary emitters [30], but they run into a number of tricky issues, such as poor spectral stability and color repeatability, and fabrication complexity [31–34]. To address these issues, creating a single-molecule white-light emission (SMWLE) material is the most effective way. Yang et al. harvested a SMWLE material with the CIE (CIE: Commission International de l'Eclairage) coordinates of (0.31, 0.33) by precisely controlling the doping ratio of 2-chlorothioxanthone and polymethyl methacrylate, which is composed of monomer fluorescence, monomer RTP and aggregate RTP emission [35]. Zhao et al. developed an *o*-carborane-based SMWLE material by high-purity complementary color induced by the charge-transfer state (CT) state and the localized state (LE) state emission, whose emission efficiency is up to 67% [36]. Tang et al. constructed a SMWLE material by tuning the degree of crystallization of 1,2,3,4-tetraphenyloxazoliums with different counterions, which can change intensity ratio blue fluorescence and yellow RTP [37]. Li et al. obtained a SMWLE by combining monomer and excimer emission and tuning their luminous proportion [38]. However, highly efficient SMWLE still faces significant challenges in terms of molecular design and device architecture.

Aim at the above-mentioned problems, here two phenothiazine based luminogens named PtzIP and PtzIPCN were designed and synthesized respectively, whose phenothiazine unit and imidazolopyridine/cyanophenyl imidazolopyridine unit were used as electron donor and electron acceptor in turn. Crystal PtzIP exhibits a blue shift of 25 nm before/after grinding, but the mechanochromism is irreversible by heating and solvent fuming. Of note, crystal PtzIP shows RTP with emission maxima at 613 nm, and its emission maxima can be tuned by crushing and grinding. In contrast, crystal PtzIPCN exhibits mechanochromism and RTP inertness. When DCM solution of PtzIP and PtzIPCN were cooled to liquid nitrogen temperature, the bright afterglows confirm phosphors nature of two luminogens after switching off UV lamp. To enhance the phosphorescence performance of two compounds, host-guest doping systems were constructed by dissolving PtzIP/PtzIPCN and PMMA in DCM according to weight ratios of 1:10 and 1:100. The results indicate PtzIP and PtzIPCN present concentration dependent fluorescence and phosphorescence emission, with RTP lifetime of 48.93–185.31 ms and afterglow of 0.2–2.0 s. More importantly, PtzIP shows near-white emission with the CIE coordinates of (0.33, 0.25) by adjusting the doping ratio between PtzIP and PMMA. Subsequently, PtzIP and PtzIPCN were doped respectively into *p*-fluorobenzophenone (F-BP) substrates at weight ratios of 1:10000 to 1:10, and RTP lifetime of PtzIPCN further were extended to 216.63 ms. Finally, a series of anti-counterfeiting patterns and information encryption were constructed based on host-guest doping. More importantly, the underlying mechanism behind phosphorescence has been explored in detail by photophysical testing, crystal analysis, and theoretical calculations.

2. Results and discussion

2.1. Photophysical and ML properties

PtzIP and PtzIPCN were prepared and purified by multi-step synthesis reactions, column chromatography, and recrystallization (Scheme S1), whose structures were thoroughly characterized by ^{1}H NMR, ^{13}NMR, and HR- MS (Figs. S13–18), and the corresponding single crystals were obtained by solvent diffusion from *n*-hexane to DCM solution of PtzIP/PtzIPCN. Notably, absorption maxima of PtzIPCN compared with PtzIP shows obvious bathochromic-shift, confirming the introduction of cyanobenzene can enlarge molecular π-conjugation (Fig. S1a), but their emission spectra give an opposite trend (Figs. S1b and S1d), illustrating the more distorted molecular conformation in excited state for PtzIPCN than PtzIP. In various solvents, PtzIP rendered dual band fluorescence emission corresponding to weak local (LE) and strong intramolecular charge transfer (ICT) states respectively, which was further confirmed by different excitation spectra (Fig. S1c). Compared with PtzIP, PtzIPCN shows enhanced ICT effect due to assembly of electron-withdrawing functional group, whose dual band fluorescence emission only can be observed in *n*-hexane and DCM, and the LE state emission is weak in comparison to the ICT emission. To investigate ICT effect of PtzIP and PtzIPCN, the time-dependent density functional theory (TD-DFT) calculations were carried out. The highest occupied molecular orbitals (HOMO) of PtzIP and PtzIPCN mainly locate on phenothiazide unit, whereas the lowest unoccupied molecular orbitals (LUMO) are distributed on other parts beyond the carbazole unit or *N*-phenylcarbazole unit, further confirming ICT effect of PtzIP and PtzIPCN. Note that the electron cloud density of PtzIP on HOMO and LUMO has a slight overlap, but complete separation for PtzIPCN, indicating stronger ICT effect for PtzIPCN than PtzIP (Fig. 1b). Under ultraviolet radiation of 365 nm, crystals PtzIP and PtzIPCN appear light yellow and earthy yellow in sequence. By grinding, PtzIP with mechanochromic activity gives a color contrast visible to the naked eyes from earthy yellow to deep blue, while PtzIPCN shows mechanochromism inertness (Fig. 2b). Furthermore, ground PtzIP samples perform irreversible mechanochromism by heating and solvent fuming (Fig. 2c). To reveal the underlying mechanism of distinct mechanochromism between crystal PtzIP and PtzIPCN, X-ray diffraction (XRD) signals were tested and analyzed (Fig. 2d). For PtzIP, grinding causes severe recession of two strong XRD signals at 24.8° (3.586 Å) and 23° (3.869 Å), which approaches intermolecular π-π stacking (3.222 Å). Thereby mechanochromism of PtzIP is attributed to the reduced intermolecular π-π stacking, leading to blue-shift of emission maxima from 475 nm to 450 nm, while irreversibility of mechanochromism is due to intermolecular π-π stacking cannot be repaired by heating and solvent fuming (Fig. 1c). By contrast, PtzIPCN presents dense and strong XRD signals before/after grinding, indicating stronger crystallizability for PtzIPCN than PtzIP, which should take responsible for mechanochromism inertness (Fig. S8). Interestingly, the RTP peak of crystal PtzIP is up to 613 nm and exhibits adjustable phosphorescence by crushing and grinding, and their RTP characteristics have been confirmed by phosphorescence lifetime (2e and 2f), whereas RTP of PtzIPCN cannot be detected by instruments (Fig. 2a). Significantly, RTP materials with phosphorescence peak >600 nm and mechanochromic activity are rarely reported in literatures. To reveal the mechanisms behind the above phenomena, phosphorescence spectra of PtzIPCN and PtzIP were tested in DCM solution at 77 K (Fig. S3). The results indicate both PtzIPCN and PtzIP are phosphors in nature, the corresponding phosphor emission peaks are 560 nm and 515 nm in turn. For comparison, crystal PtzIP displays a bathochromic shift of nearly 100 nm in emission maxima of RTP compared with its DCM solution at 77 K, which derives from aggregates and monomers of PtzIP in turn. By crushing, PtzIP gives two RTP peaks located at 530 nm and 560 nm respectively. The former is close to monomer phosphorescence

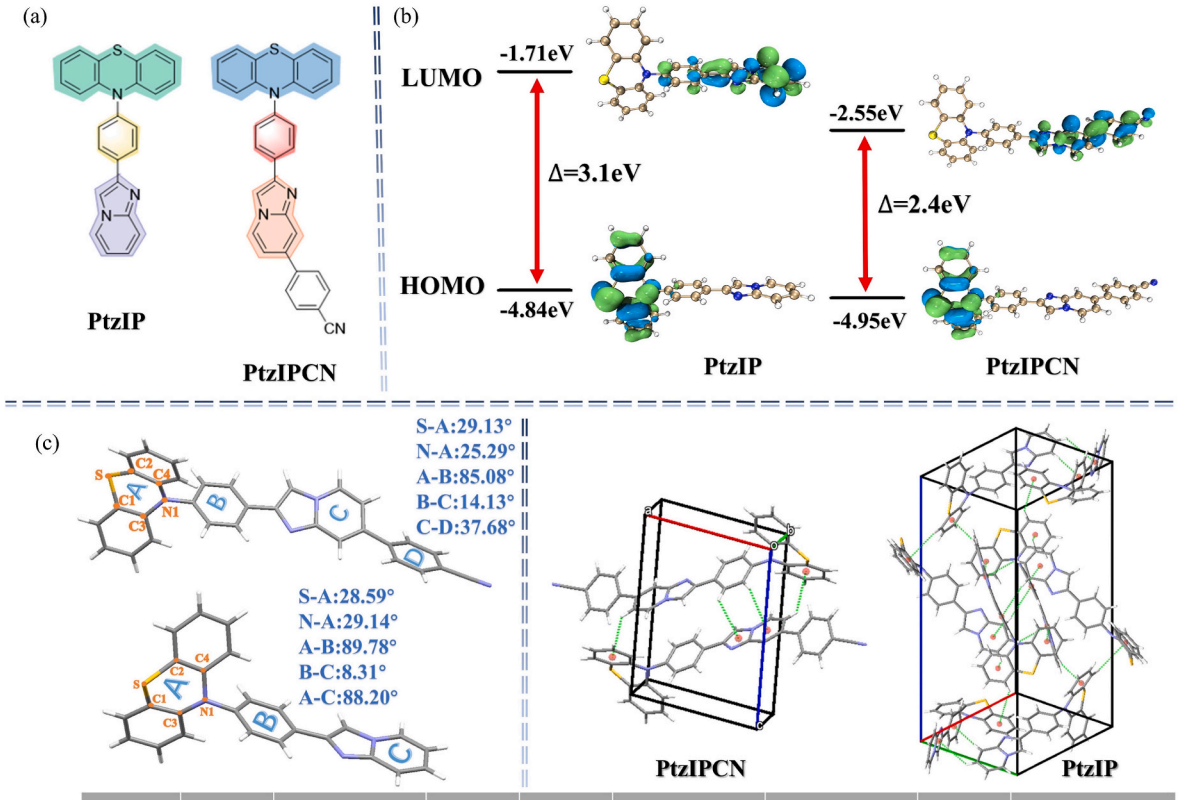

	C-H…S	C-H…C	C-H…H	C-H…N	C-H…π	C…C	C…S	π –π stacking
PtzIP	2.902	2.756, 2.890, 2.781, 2.873, 2.836, 2.800, 2.608, 2.878	2.233		3.256, 3.277, 3.337, 2.769, 2.938, 2.918, 3.249, 3.249,	3.222	3.426	3.681, 3.684, 3.838, 3.678, 3.375, 3.422, 3.694, 3.683
PtzIPCN	2.876	2.813, 2.826, 2.828, 2.773, 2.794		2.610, 2.587	2.942, 3.063, 3.230	3.307, 3.390, 3.360		3.578, 3.408, 3.602, 3.381, 2.976, 2.994, 3.577

Fig. 1. (a) The molecular structures of PtzIP and PtzIPCN. (b) The HOMO and LUMO of PtzIP and PtzIPCN. (C) Molecular conformation and intermolecular interactions of crystals PtzIP and PtzIPCN.

(515 nm), whose bathochromic-shift may come from more intense exciton relaxation at room compared with 77 K, while the latter belongs to aggregates, which yields 60 nm blue shift in comparison to the pristine crystal. As the reported literatures, crushing can lead to "disaggregation" process in fracture surface, and thereby produce monomer phosphorescence. For aggregates, the small crystal size shortens the molecular delocalization path, reducing non-radiation energy loss, which results in blue shift of phosphorescence emission. By grinding, monomer phosphorescence becomes shoulder peak, while aggregate phosphorescence red shifts to 585 nm from 560 nm due to enhanced intermolecular interactions and formation of different aggregates. Generally, RTP originates from the LE excited state of luminogen, and the triplet exciton is vulnerable to triplet oxygen, therefore small molecule RTP materials with adjustable phosphorescence wavelength are difficult to discover. Next, the internal mechanism of mechanochromism and RTP are further revealed by crystal analysis (Fig. 1c). Both PtzIP (CCDC 2291729) and PtzIPCN (CCDC 2291730) exhibit highly twisted molecular configurations and saddle shaped phenothiazide structural units, and the corresponding dihedral angles between the S plane (S, C1 and C2) and ring A (C1, C2, C3 and C4 are defined as ring A) are 29.13° and 28.59° in turn, while the angles between the N plane (N1, C3 and C4) and ring A are 25.29° and 29.14° separately. For PtzIP, one cell unit contains seven PtzIP molecules, and the dihedral angles are 89.75°, 8.31° and 88.20° in turn for ring A-B, B–C and A-C. Twenty-four intermolecular hydrogen bonds and weak interaction are formed between a molecule and its surrounding molecules (Fig. S5). More importantly, intermolecular π-π stacking can be observed between phenothiazide units, as well between phenothiazide unit and benzene bridges (Figs. S6–S7), corresponding to XRD diffraction signals at 24.8° and 23° very well. By contrast, two PtzIPCN molecules can be found in one cell unit, presenting weaker intermolecular hydrogen bonds and interactions but stronger intermolecular π-π stacking in comparison to PtzIP (Fig. 1c). Therefore, PtzIPCN shows excellent crystallizability mainly due to the strong intermolecular π-π stacking, leading to deprivation of mechanochromism. We know that the excellent crystallizability and intermolecular π-π stacking are usually beneficial for stabilizing triplet excitons, so the absence of RTP for crystal PtzIPCN cannot be simply attributed to non-radiative deactivation of triplet excitons, which will be further discussed in detail by theoretical calculations.

2.2. PMMA doped system

Considering the phosphorescence characteristics of PtzIP and PtzIPCN at 77 K, the host-guest doping systems were constructed by dissolving PtzIP/PtzIPCN and PMMA in DCM according to weight ratios of 1:10 and 1:100, then 1% and 10% PtzIP/PtzIPCN doped films named as 1%PtzIP@PMMA, 10%PtzIP@PMMA, 1%PtzIPCN @PMMA and 10%

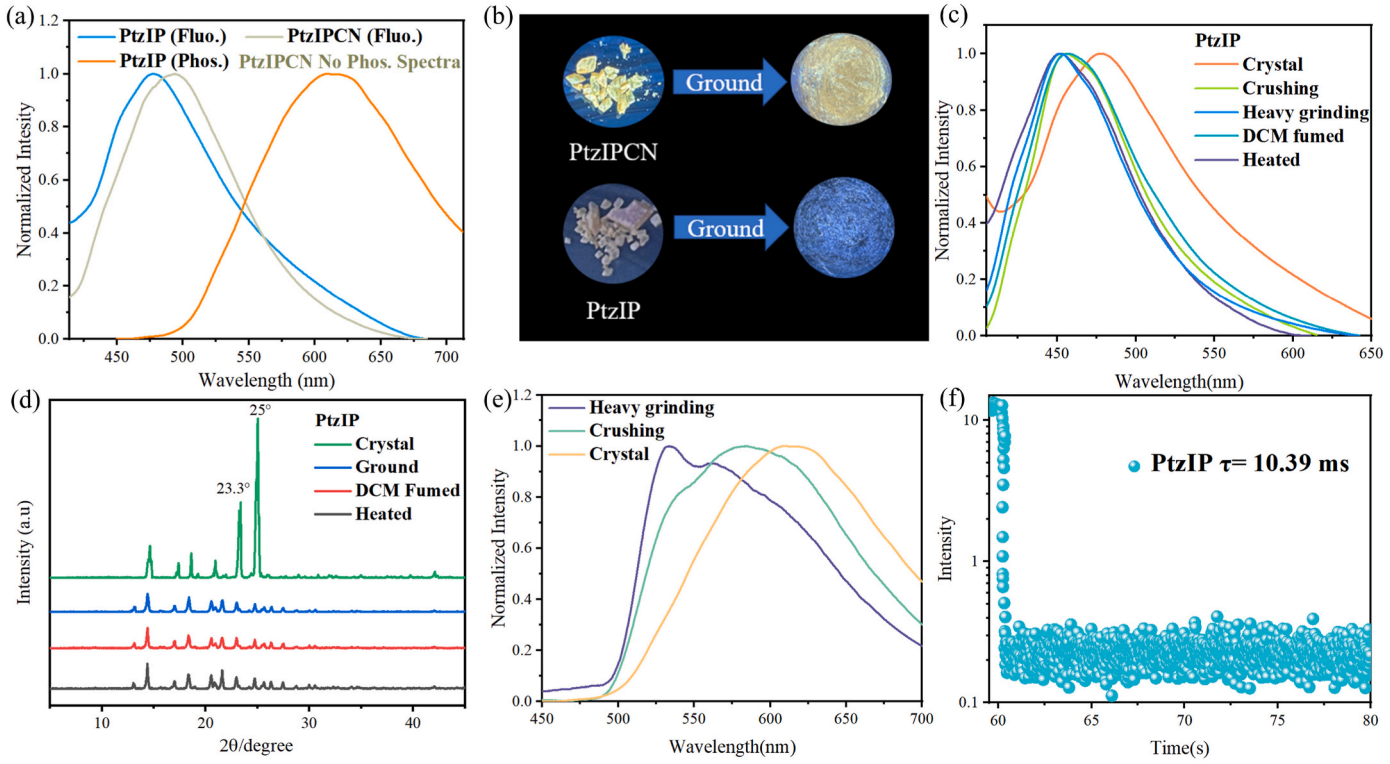

Fig. 2. (a) Fluorescence and phosphorescence emission spectra of crystals PtzIP and PtzIPCN. (b) Comparison pictures of crystals PtzIP and PtzIPCN before and after grinding. (c) Fluorescence spectra of PtzIP in different states (λ_{ex}: 340 nm). (d) Corresponding X-ray diffraction patterns and (e) phosphorescence emission spectra of PtzIP in different states (delayed time: 1 ms, λ_{ex}: 365 nm). (f) Time-resolved phosphorescence decay curves of crystal PtzIP excited at 365 nm.

PtzIPCN@PMMA were prepared by literature method. Switching on UV lamp, 1%PtzIP@PMMA and 10%PtzIP@PMMA films emit green fluorescence, whose dual band fluorescence emission maxima are located at 396 nm, 527 nm, 460 nm, and 510 nm respectively (Fig. 3a and 3c). By comparison, emission maxima at 396 nm and 460 nm should come from PtzIP monomers and aggregates separately, while emission peaks at 527 nm and 510 nm are very close to RTP emission maxima at 548 nm and 527 nm, which should belong to triplet state emission, and the corresponding RTP lifetimes increase to 48.93 ms and 56.84 ms from 7.63 ms of crystal, yielding 0.2 s and 0.4 s afterglow after UV lamp is turned off (Fig. 3a and 3b). Notably, PMMA matrix can inhibit energy loss caused by molecular motion, but inability to diffuse oxygen, and thereby the presence of RTP needs undergo UV irradiation of 30–60 s to remove triplet oxygen. Different from PtzIP doped films, both 1% PtzIPCN@PMMA and 10%PtzIPCN@PMMA films yield single fluorescence and phosphorescence peaks (Fig. 3d), and Stokes shifts between RTP and fluorescence emission maxima significantly decrease, which is consistent with the enhanced ICT effect for PtzIPCN than PtzIP, leading to the reduced ΔE_{ST}. Furthermore, small ΔE_{ST} (0.22 eV) is beneficial for generating more triplet excitons, which can take responsible for durable RTP lifetime (185.31 ms) and improved quantum efficiency (0.08) for 1%PtzIPCN@PMMA film. With the doping concentration further increases, 10%PtzIPCN@PMMA film gives inferior RTP lifetime (49.49 ms) and quantum efficiency (0.06), whose ΔE_{ST} decreases to 0.19 eV, which can boost triplet's exciton generation and resulting collision quenching (Fig. 3b). It is noteworthy that afterglow of 1% PtzIPCN@PMMA and 10%PtzIPCN@PMMA films extend to 1 s and 2 s in turn (Fig. 3a). Overall, RTP performance of PtzIP and PtzIPCN can be effectively improved by PMMA doping, and PtzIP and PtzIPCN present concentration dependent fluorescence and phosphorescence emission in doping films possibly due to different intermolecular interactions and molecular conformations. Based on the dual band emission of 1% PtzIP@PMMA and 10%PtzIP@PMMA films, we attempt to obtain a SMWLE material by adjusting the doping ratio (Fig. 3e-g). When the doping ratio between PtzIP and PMMA is 15%, the doping film presents single-molecule near-white light emission, with the (CIE: Commission International de I'Eclairage) CIE coordinates of (0.33, 0.25).

2.3. F-BP doped system

Owing to low melting temperature, excellent crystallinity, and boosting the intersystem crossing (ISC) between singlet and triplet exciton, diphenylmethanone and its derivatives are usually chosen as host to improve RTP of guest. Here, F-BP/PtzIP and F-BP/PtzIPCN doping systems were constructed and optimized. When the doping weight ratio between PtzIP/PtzIPCN and F-BP is 1:10000, phosphorescence emission of F-BP/PtzIP is almost unaffected by trance PtzIP, but F-BP/PtzIPCN shows significantly enhanced emission intensity at 520 nm, which should be attributed to better phosphorescence performance for PtzIPCN monomer than PtzIP monomer. With the increasing doping concentration from 1: 1000 to 1:10, multiple phosphorescence peaks mainly coming from host transform into a single RTP peak, accompanied by continuous reduction of phosphorescence intensity (Figs. S10a–S10c). From this, the optimal doping ratio of host-guest is determined as 1000:1, and we speculate that phosphorescence emission of two doping systems derive from guest rather than host. Under 365 nm UV lamp, F-BP/PtzIP and F-BP/PtzIPCN emit light blue and yellow fluorescence respectively, then present dimmed green and bright yellow afterglow in turn when UV lamp is switched off, which last separately 0.5 s and 1.5 s, corresponding to phosphorescence lifetimes of 101.21 ms and 216.63 ms in sequence (Fig. 4a and g). The XRD patterns show that F-BP/PtzIP and F-BP/PtzIPCN still maintain crystalline states, which matches with XRD patterns of F-BP very well, demonstrating the ordered intermolecular arrangement and stacking of host material are not destroyed after doping (Fig. S11). Compare the absorption spectra between F-BP, PtzIP/PtzIPCN, and F-BP/PtzIP or F-BP/PtzIPCN, excimer is

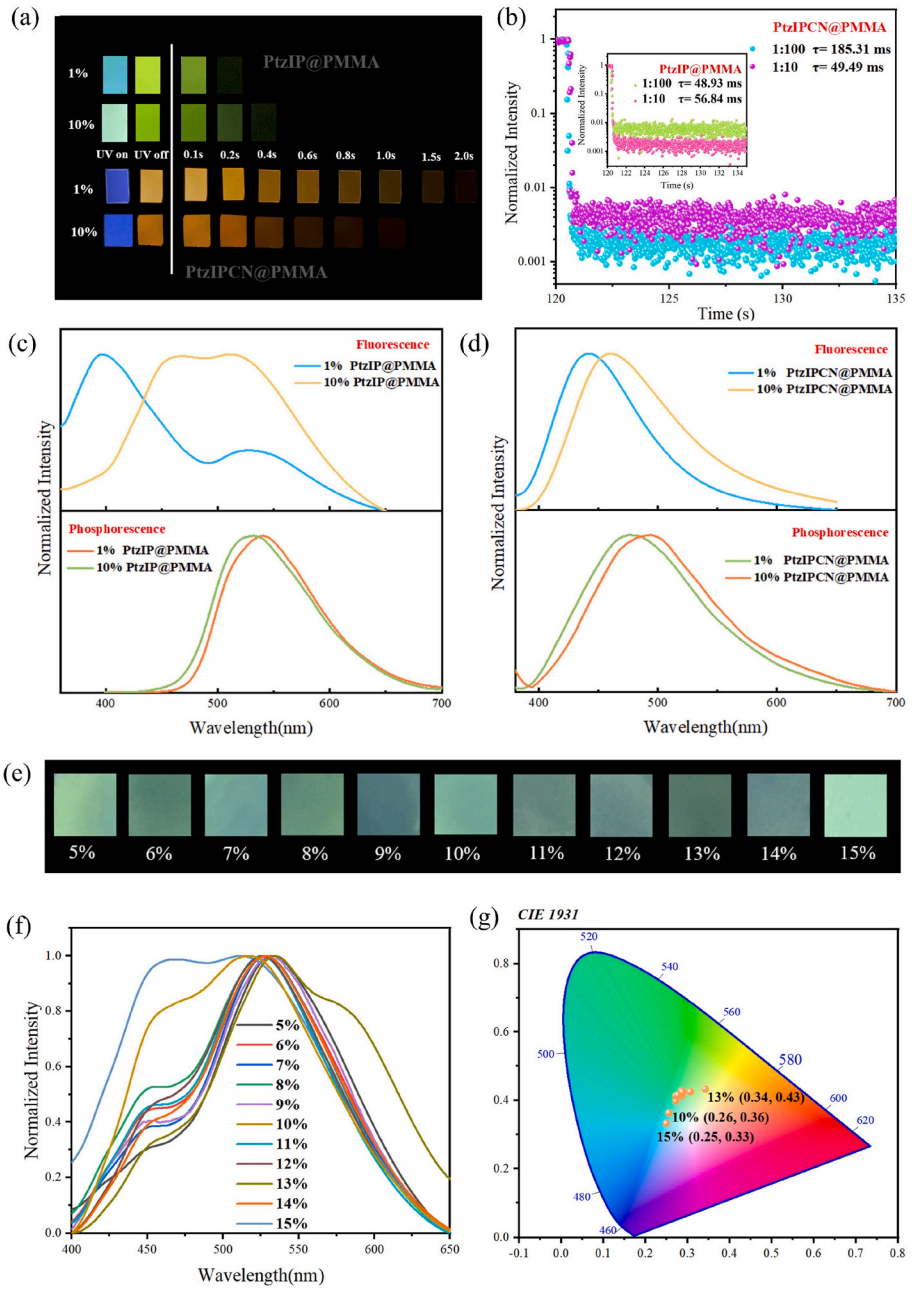

Fig. 3. (a) Photograph of PtzIP@PMMA and PtzIPCN@PMMA films under UV light. (b) Time-resolved phosphorescence decay curves of PtzIP@PMMA and PtzIPCN@PMMA films. (c) Fluorescence and phosphorescence spectra of PtzIP@PMMA films and (d) PtzIPCN@PMMA films at different doping concentrations (delayed time: 1 ms, λ_{ex}: 365 nm). (e) Photograph of PtzIP@PMMA films at different doping concentrations under UV light. (f) Phosphorescence spectra and (g) CIE chromaticity coordinates of PtzIP@PMMA films at different doping concentrations (delayed time: 1 ms, λ_{ex}: 365 nm).

excluded due to absence of new absorption peaks (Fig. 4d and S10d).

It is worth noting that there is some overlap between the emission spectra of F-BP and the absorption spectra of PtzIPCN at 375–450 nm (Fig. 4e), which may trigger Föster resonance energy transfer (FRET). To explore phosphorescence mechanism of the two doping systems, their phosphorescence intensity at different excitation wavelength were provided. As shown in Fig. 4f and Fig. S10f, two doping systems show the strongest phosphorescence intensity under 365 nm excitation, followed by 430 nm and 280 nm. Combined with absorption spectra of F-BP, PtzIP/PtzIPCN, and the two doping systems, phosphorescence mechanism of the two doping systems should be excitation of guest, but not for FRET from host to guest, as well host sensitized luminescence. Compared with crystal PtzIPCN, crystal PtzIP shows better phosphorescence performance, but the two doping systems give an opposite result. In order to understand the mechanism of behind the above phenomenon in detail, energy levels and spin-orbit couplings (ξ) between singlet and triplet states of F-BP, PtzIP, and PtzIPCN were calculated by extracting single crystal data, whose ground and excited state structures were further optimized by using time-dependent density functional theory (DFT) at the PBE0-def2svp level (Fig. 4h–j). It can be seen from Fig. 4h–j that the S_1 and T_1 of PtzIP monomer are 3.20 eV and 1.94 eV respectively, but the S_1 and T_1 of the dimer move to 3.18 eV and 1.95 eV, indicating the reduced ΔE_{ST} from monomer (1.26 eV) to dimer (1.23 eV), which is accompanied by increasing $\xi(S_1 \rightarrow T_1)$ from 0.010 cm^{-1} to 0.017 cm^{-1}, as well $\xi(T_1 \rightarrow S_0)$ from 0.10 cm^{-1} to 0.60 cm^{-1}. Different from PtzIP, ΔE_{ST} of PtzIPCN sharply decreases from monomer (1.12 eV) to dimer (0.80 eV), and $\xi(S_1 \rightarrow T_1)$ and $\xi(T_1 \rightarrow S_0)$ drop to 0. In theory, small ΔE_{ST} and large $\xi(S_1 \rightarrow T_1)$ are beneficial for promoting ISC. The

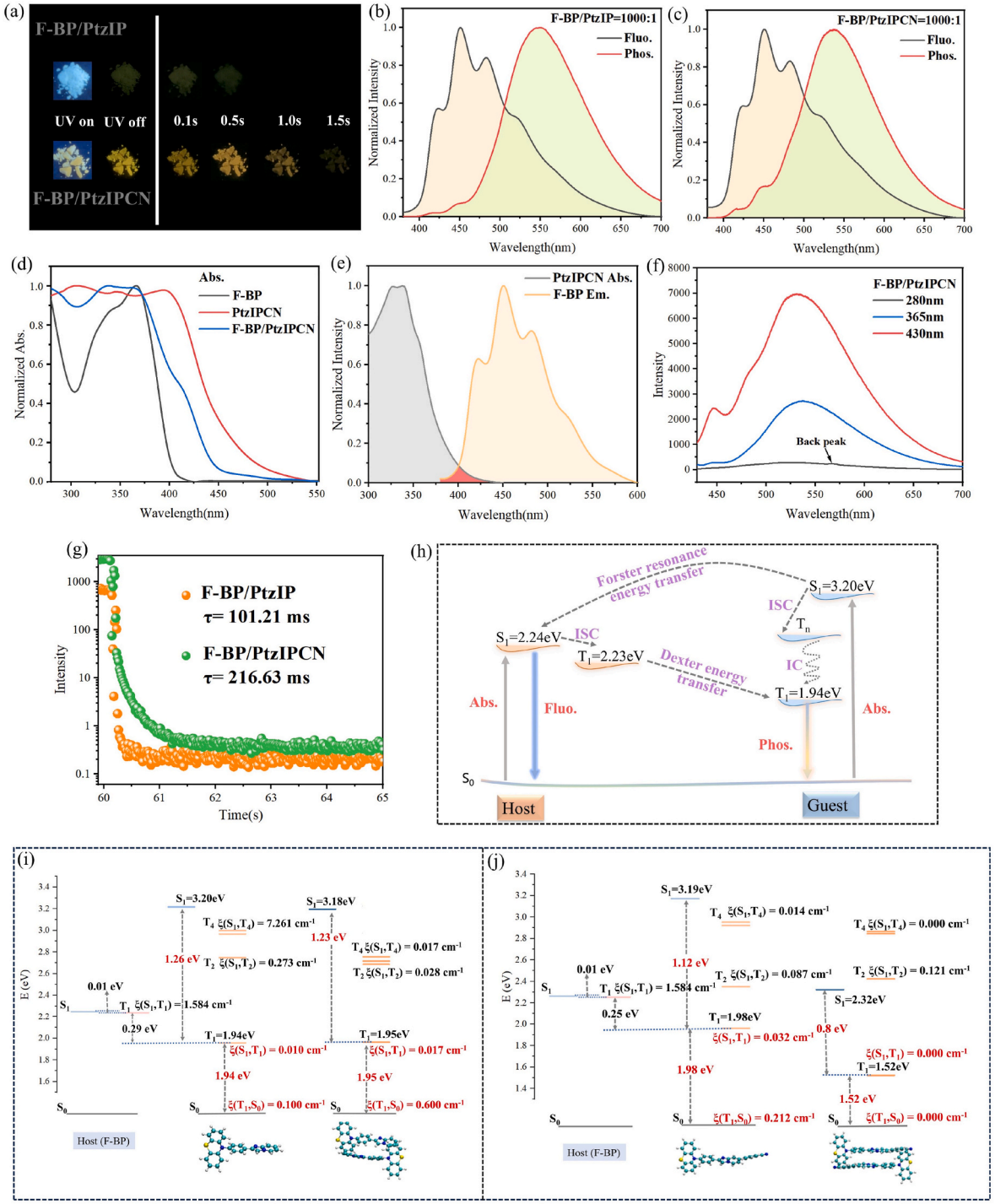

Fig. 4. (a) Photographs under 365 nm light irradiation and turning off the light irradiation of F-BP/PtzIP and F-BP/PtzIPCN at optimal doping concentration. (b) Fluorescence and phosphorescence spectra of F-BP/PtzIP and (c) F-BP/PtzIPCN at optimal doping concentration (delayed time: 1 ms, λ_{ex}: 365 nm). (d) UV absorption spectra of F-BP, PtzIPCN, and F-BP/PtzIPCN in solid states. (e) Fluorescence spectra of F-BP in solid states and UV absorption spectra of guest PtzIPCN in dichloromethane solution (1×10^{-5} M). (f) Delayed fluorescence emission spectra of F-BP/PtzIPCN doped materials at different excitation wavelengths. (g) Time-resolved phosphorescence decay curves of doping systems. (h) Proposed photophysical processes in host-guest doping systems. (i) The energy levels of the PtzIP monomer, dimer and F-BP. (j) The energy levels of the PtzIPCN monomer, dimer and F-BP.

calculation results combined with theoretical analysis suggest the following conclusion: 1) RTP performance of dimer PtzIP is superior to that of monomer PtzIP, but RTP performance of monomer PtzIPCN is better than that of dimer PtzIPCN, which corresponds to 10% PtzIP@PMMA films showing a longer RTP lifetime than 1% PtzIP@PMMA, but RTP lifetime of 1% PtzIPCN@PMMA films is longer than 10% PtzIPCN@PMMA films. 2) Based on smaller ΔE_{ST}, as well bigger $\xi(S_1 \rightarrow T_1)$ and $\xi(T_1 \rightarrow S_0)$ for dimer PtzIP than dimer PtzIPCN, it can be inferred that crystal PtzIP relative to crystal PtzIPCN is more prone to producing RTP, which is consistent with the experiment results. 3) F-BP/PtzIPCN shows better phosphorescence performance than F-BP/PtzIP, which should be because PtzIPCN/PtzIP is dispersed in the form of monomers rather than aggregates in two doping systems. Compared with PtzIP monomers, PtzIPCN monomers show the reduced ΔE_{ST} and

the increased $\xi(S_1 \rightarrow T_1)$ and $\xi(T_1 \rightarrow S_0)$, which is conducive to phosphorescence emission of F-BP/PtzIPCN. 4) F-BP has tiny ΔE_{ST} (0.01 eV) and $\xi(S_1 \rightarrow T_1)$ of 1.584 cm^{-1}, what is more, its T_1 (2.23 eV) state locate between S_1 and T_1 of PtzIP and PtzIPCN, which contributes to reduce ΔE_{ST} and boost Dexter energy transfer (DET) from T_1 state of F-BP and to the T_1 state of PtzIP and PtzIPCN, generating more triplet excitons. Besides, PtzIP (3.20 eV) and PtzIPCN (3.19 eV) have higher the energy levels at S_1 state than F-BP (2.24eV), leading to the energy transfer from S_1 states of PtzIP and PtzIPCN and to the S_1 state of F-BP. Thereby, the phosphorescence emission processes of F-BP/PtzIP and F-BP/PtzIPCN are outlined (Fig. 4h). Under ultraviolet radiation of 365 nm, host and guest are excited to S_1 state from S_0 state. Owing to appropriate $\xi(S_1 \rightarrow T_1)$ and small ΔE_{ST} for F-BP, the singlet exciton of F-BP transfers to its T_1 state by ISC, which subsequently transfer to T_1 state of PtzIP/PtzIPCN by the DET process due to the lower T_1 state energy level for PtzIP/PtzIPCN than F-BP. Finally, T_1 state exciton of PtzIP/PtzIPCN backs to S_0 state, emitting bright phosphorescence of PtzIP/PtzIPCN [39]. Due to the inability to obtain the fluorescence emission spectra of PtzIP/PtzIPCN monomer in F-BP/PtzIP and F-BP/PtzIPCN systems, we try to analyze the FRET process by fluorescence emission spectra of 1% PtzIP@PMMA (Fig. 3c) and 1% PtzIPCN@PMMA (Fig. 3d) films, as well absorption spectra of crystal F-BP (Fig. 4d). Obviously, there is a significant overlap between absorption spectra of crystal F-BP and emission spectra of PtzIP, but not for PtzIPCN. Therefore, the singlet exciton of PtzIP can transfer to S_1 state of F-BP by the FRET process, and then yield RTP by ISC, DET, and radiative transition of $T_1 \rightarrow S_0$ [40,41]. In addition, there are two triplet excited states (T_2 and T_4) below the S_1 state for PtzIP monomer, which is beneficial to boost the rapid generation of triplet excitons due to appropriate $\xi(S_1 \rightarrow T_2)$, $\xi(S_1 \rightarrow T_4)$, and ΔE_{ST} (Fig. 4i). By contrast, the FRET and ISC processes are weak for PtzIPCN monomer because of negligible spectral overlap, small $\xi(S_1 \rightarrow T_2)$ and $\xi(S_1 \rightarrow T_4)$, as well as large ΔE_{ST} (Fig. 4j). Unfortunately, theoretical calculations cannot explain the shift of RTP emission maxima for crystal PtzIP before/after grinding, which may not only involve monomers and aggregates, but also molecular conformation and complex intermolecular interactions.

3. Applications

Based on different luminescent properties of PtzIP and PtzIPCN in doping films, digital encryption patterns were designed by selecting 1% PtzIP@PMMA, 10%PtzIP@PMMA and 10%PtzIPCN@PMMA films, which was successfully constructed by using the same "lightning'' template and different arrangement modes (Fig. 5a). Switching off UV lamp, green "lightning'' patterns constructed with 1%PtzIP@PMMA and 10%PtzIP@PMMA are set to 1, while brown "lightning'' patterns coming from 1%PtzIPCN@PMMA and 10%PtzIPCN@PMMA are set to 0. Taking the first row as an example, "01000011" can be read out, thus obtaining a set of permutation encryption passwords. By comparing the standard decryption groups (Fig. S12), we finally solve the three groups of permutation passwords as "GUT". However, 1%PtzIP@PMMA and 10%PtzIP@PMMA films appear light blue and warm white color respectively under 365 nm UV irradiation, while 1%PtzIPCN@PMMA and 10%PtzIPCN@PMMA films are deep blue, which cannot provide correct information. Under sunlight, 1%PtzIP@PMMA, 10% PtzIP@PMMA and 1%PtzIPCN@PMMA films are difficult to distinguish due to similar light yellow, thereby true information cannot be correctly read. In addition, a series of anti-counterfeiting patterns were designed and prepared based on different afterglow lifetime of host-guest doping systems (Fig. 5b). Firstly, the porous filter papers were immersed in solution of molten F-BP, and then dried in the air for 30 min. Secondly, PtzIP and PtzIPCN were dissolved respectively in DCM solution and used as ink. Finally, four weather patterns named as "sunny", "cloudy", "overcast" and "shower" were draw on the filter paper. Under solar radiation, no trace of depiction can be observed on the filter paper, but four types of weather are clearly visible under a 365 nm ultraviolet lamp. When the ultraviolet lamp is turned off, four weather patterns are still visible, but "overcast" and "shower" are brighter than "sunny" and "cloudy". Owing to stronger and more persistent RTP for F-BP-PtzIPCN than F-BP-PtzIP doping systems, only "sunny" and "cloudy" can be perceived after 1 s. From the imperceptibility in the sunlight, to four weather patterns containing false information, and finally to the real "overcast" and "shower", high-level anti-counterfeiting patterns are successfully constructed.

4. Conclusions

In summary, two new luminogens named PtzIP and PtzIPCN were prepared and characterized, whose luminescent properties were investigated in detail by photophysical performance testing, crystal analysis, and theoretical calculations. Compared with PtzIP, PtzIPCN shows bathochromic-shift absorption spectra and hypsochromic shift emission spectra in various solvents due to enlarge molecular π-conjugation and more twisted excited state molecular conformation. XRD experiments reveal that mechanochromism of PtzIP is attributed to phase transition from crystalline to amorphous state, whereas mechanochromism inertness of PtzIPCN is due to excellent crystallinity. Furthermore, XRD experiments and crystal analysis confirm that grinding destroys intermolecular π-π stacking of crystal PtzIP, leading to blue-shift (25 nm) of emission maxima. Moreover, PtzIP shows tunable RTP from 613 nm to 530 nm and 560 nm, then to 540 nm and 585 nm by crushing and grinding, which is ascribed to external mechanical forces changing the phosphorescence intensity ratio between monomers and aggregates, as

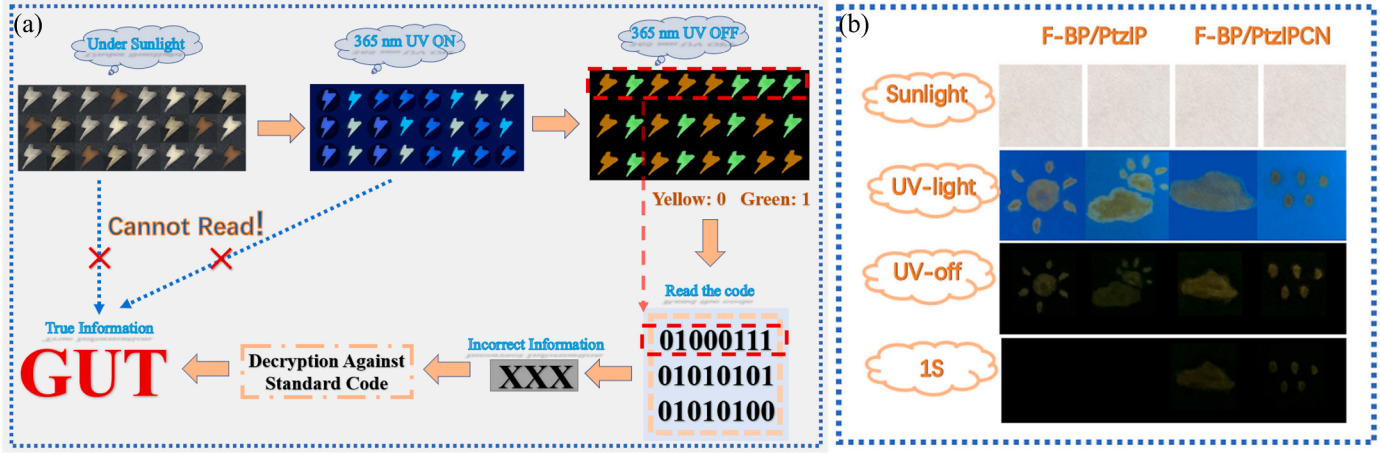

Fig. 5. Anti-counterfeiting application by using (a) PtzIP@PMMA and PtzIPCN@PMMA films, (b) the F-BP/PtzIP and F-BP/PtzIPCN doping systems.

well intermolecular interactions, and molecular conformation. By PMMA doping, RTP lifetimes of 1%PtzIP@PMMA and 10% PtzIP@PMMA films increase to 48.93 ms and 56.84 ms respectively, while 1%PtzIPCN@PMMA and 10%PtzIPCN@PMMA films give RTP lifetimes of 185.31 ms and 49.49 ms in turn, demonstrating PMMA doping can effectively suppress non-radiative energy decay of triplet excitons, as well change unfavorable intermolecular arrangement and stacking modes of crystal PtzIPCN. Different from single band fluorescence emission of 1%PtzIPCN@PMMA and 10%PtzIPCN@PMMA films, 1%PtzIP@PMMA (396 nm and 527 nm) and 10%PtzIP@PMMA (460 nm, and 510 nm) films present dual band fluorescence emission, whose high energy emission bands come from fluorescence emission, but low energy emission bands belong to phosphorescence. Furthermore, a single-molecule near-white light emission material with the CIE coordinates of (0.33, 0.25) is achieved by adjusting the doping ratio between PtzIP and PMMA. In PMMA doping films, PtzIP and PtzIPCN present concentration dependent fluorescence and phosphorescence emission possibly due to different intermolecular interactions and molecular conformations. Compared with PMMA doped systems, RTP performance of F-BP/PtzIP and F-BP/PtzIPCN hardly show obviously improvement, which may be because ΔE_{ST} of the two doping systems is still much higher than 0.57 eV. Theoretical calculation results reveal that RTP performance of PtzIP and PtzIPCN monomers and dimers have significant difference, which should take responsible for doping concentration dependent phosphorescence lifetime and high-contrast RTP between PtzIP and PtzIPCN in crystalline and doping systems. In addition, theoretical calculation also indicates the phosphorescence emission processes of F-BP/PtzIP and F-BP/PtzIPCN possibly involve FRET from guest to host and DET from host to guest. Based on different luminescent properties of PtzIP and PtzIPCN in the doping systems, a series of high-level digital encryption and anti-counterfeiting patterns are successfully constructed. The work not only provides a novel material with mechanochromism, tunable RTP, and SMWLE properties, as well two long-lived RTP doping systems, but also contributes to boost deep understanding of the structure-property relationships.

CRediT authorship contribution statement

Jianmei Guo: Synthesis, Investigation, Data acquisition, Writing – original draft, preparation. **Chenwei Hu:** Data acquisition, Writing – original draft, preparation. **Jiaqi Liu:** Data acquisition. **Yongtao Wang:** Conceptualization, Writing – review & editing. **Lei Ma:** Writing – review & editing.

Declaration of competing interest

The authors declare that they have no known competing financial interests or personal relationships that could have appeared to influence the work reported in this paper.

Data availability

No data was used for the research described in the article.

Acknowledgment

This work was supported by the Guangxi Natural Science Foundation (Grant No. 2020GXNSFAA159147), the National Natural Science Foundation of China (Grant No. 21766030 and 21566034) and the Guilin University of Technology Research Fund (Grant No. GUTQDJJ2019038 and GUTQDJJ2018052).

Appendix A. Supplementary data

Supplementary data to this article can be found online at https://doi.org/10.1016/j.dyepig.2023.111760.

References

[1] Xiong S, Xiong Y, Wang D, Pan Y, Chen K, Zhao Z, Wang D, Tang BZ. Achieving tunable organic afterglow and UV-Irradiation-Responsive ultralong room-temperature phosphorescence from pyridine-substituted triphenylamine derivatives. Adv Mater 2023;35:2301874.
[2] Dou X, Zhu T, Wang Z, Sun W, Lai Y, Sui K, Tan Y, Zhang Y, Yuan WZ. Color-tunable, excitation-dependent, and time-dependent afterglows from pure organic amorphous polymers. Adv Mater 2020;32:2004768.
[3] Wang Y, Gao H, Yang J, Fang M, Ding D, Tang BZ, Li Z. High performance of simple organic phosphorescence host-guest materials and their application in time-resolved bioimaging. Adv Mater 2021;33:2007811.
[4] Wang XF, Xiao H, Chen PZ, Yang QZ, Chen B, Tung CH, Chen YZ, Wu LZ. Pure organic room temperature phosphorescence from excited dimers in self-assembled nanoparticles under visible and near-infrared irradiation in water. J Am Chem Soc 2019;141:5045–50.
[5] Ma X, Wang J, Tian H. Assembling-induced emission: an efficient approach for amorphous metal-free organic emitting materials with room-temperature phosphorescence. Acc Chem Res 2019;52:738–48.
[6] Lucenti E, Forni A, Botta C, Carlucci L, Giannini C, Marinotto D, Previtali A, Righetto S, Cariati E. H-aggregates granting crystallization-induced emissive behavior and ultralong phosphorescence from a pure organic molecule. J Phys Chem Lett 2017;8:1894–8.
[7] Ma L, Sun S, Ding B, Ma X, Tian H. Highly efficient room-temperature phosphorescence based on single-benzene structure molecules and photoactivated luminescence with afterglow. Adv Funct Mater 2021;31:2010659.
[8] Cai S, Shi H, Zhang Z, Wang X, Ma H, Gan N, Wu Q, Cheng Z, Ling K, Gu M, Ma C, Gu L, An Z, Huang W. Hydrogen-bonded organic aromatic frameworks for ultralong phosphorescence by intralayer pi-pi interactions. Angew Chem Int Ed Engl 2018;57:4005–9.
[9] Yu Z, Wu Y, Xiao L, Chen J, Liao Q, Yao J, Fu H. Organic phosphorescence nanowire lasers. J Am Chem Soc 2017;139:6376–81.
[10] El-Sayed MA. Spin—orbit coupling and the radiationless processes in nitrogen heterocyclics. J Chem Phys 1963;38:2834–8.
[11] Zhou Y, Song J, Hu Y, Cao J, Fu Y, Ma X. Stimuli-responsive room-temperature phosphorescence regulation based on molecular packing mode conversion. Dyes Pigments 2023;215:111272.
[12] Xie Y, Ge Y, Peng Q, Li C, Li Q, Li Z. How the molecular packing affects the room temperature phosphorescence in pure organic compounds: ingenious molecular design, detailed crystal analysis, and rational theoretical calculations. Adv Mater 2017;29:1606829.
[13] Ruan Z, Liao Q, Dang Q, Chen X, Deng C, Gao Z, Lin J, Liu S, Chen Y, Tian Z, Li Z. Luminous butterflies: rational molecular design to optimize crystal packing for dramatically enhanced room-temperature phosphorescence. Adv Opt Mater 2021;9:2001549.
[14] Mane SKB, Mu Y, Ubba E, Yang Z, Zhao J, Chi Z. Tuning the organic persistent room-temperature phosphorescence through aggregated states. J Mater Chem C 2019;7:15219–24.
[15] Bolton O, Lee K, Kim HJ, Lin KY, Kim J. Activating efficient phosphorescence from purely organic materials by crystal design. Nat Chem 2011;3:205–10.
[16] Zhang G, Palmer GM, Dewhirst MW, Fraser CL. A dual-emissive-materials design concept enables tumour hypoxia imaging. Nat Mater 2009;8:747–51.
[17] Zhang ZY, Chen Y, Liu Y. Efficient room-temperature phosphorescence of a solid-state supramolecule enhanced by cucurbit[6]uril. Angew Chem Int Ed Engl 2019;58:6028–32.
[18] Yang Z, Mao Z, Zhang X, Ou D, Mu Y, Zhang Y, Zhao C, Liu S, Chi Z, Xu J, Wu YC, Lu PY, Lien A, Bryce MR. Intermolecular electronic coupling of organic units for efficient persistent room-temperature phosphorescence. Angew Chem Int Ed Engl 2016;128:2221–5.
[19] An Z, Zheng C, Tao Y, Chen R, Shi H, Chen T, Wang Z, Li H, Deng R, Liu X, Huang W. Stabilizing triplet excited states for ultralong organic phosphorescence. Nat Mater 2015;14:685–90.
[20] Ding B, Ma X, Tian H. Recent advances of pure organic room temperature phosphorescence based on functional polymers. Acc Mater Res 2023. https://doi.org/10.1021/accountsmr.3c00090.
[21] Su Y, Jin X, Su J, Feng Y, Wang Q, Zhang Z, Tian H, Ma X. Radical afterglow emission harnessed by doping N, N'-Diaryl-5,10-Dihydrophenazines to epoxy resins. Adv Opt Mater 2023:2300604.
[22] Zhang H, Ma H, Huang W, Gong W, He Z, Huang G, Li BS, Tang BZ. Controllable room temperature phosphorescence, mechanoluminescence and polymorphism of a carbazole derivative. Mater Horiz 2021;8:2816–22.
[23] Qiu W, Cai X, Li M, Chen Z, Wang L, Xie W, Liu K, Liu M, Su SJ. Achieving purely organic room-temperature phosphorescence mediated by a host-guest charge transfer state. J Phys Chem Lett 2021;12:4600–8.
[24] Chen B, Zhang X, Wang Y, Miao H, Zhang G. Aggregation-induced emission with long-lived room-temperature phosphorescence from methylene-linked organic donor-acceptor structures. Chem Asian J 2019;14:751–4.
[25] Fang B, Lai L, Fan M, Yin M. Designing organic room temperature phosphorescence with ultralong lifetime by substituent modification. J Mater Chem C 2021;9:11172–9.
[26] Yue L, Yuan S, Zhang Y, Wang Y, Sun Q, Zhang H, Xue S, Yang W. Gaining new insights into trace guest doping role in manipulating organic crystal phosphorescence. J Phys Chem Lett 2021;12:11616–21.
[27] Gan N, Wang X, Ma H, Lv A, Wang H, Wang Q, Gu M, Cai S, Zhang Y, Fu L, Zhang M, Dong C, Yao W, Shi H, An Z, Huang W. Manipulating the stacking of

triplet chromophores in the crystal form for ultralong organic phosphorescence. Angew Chem Int Ed Engl 2019;58:14140–5.
[28] Liu Y, Ma Z, Liu J, Chen M, Ma Z, Jia X. Robust white-light emitting and multi-responsive luminescence of a dual-mode phosphorescence molecule. Adv Opt Mater 2020;9:2001685.
[29] Lei Y, Dai W, Guan J, Guo S, Ren F, Zhou Y, Shi J, Tong B, Cai Z, Zheng J, Dong Y. Wide-range color-tunable organic phosphorescence materials for printable and writable security inks. Angew Chem Int Ed Engl 2020;59:16054–60.
[30] Feng H-T, Zheng X, Gu X, Chen M, Lam JWY, Huang X, Tang BZ. White-light emission of a binary light-harvesting platform based on an amphiphilic organic cage. Chem Mater 2018;30:1285–90.
[31] Yang QY, Lehn JM. Bright white-light emission from a single organic compound in the solid state. Angew Chem Int Ed Engl 2014;126:4660–5.
[32] Kim SH, Park S, Kwon JE, Park SY. Organic light-emitting diodes with a white-emitting molecule: emission mechanism and device characteristics. Adv Funct Mater 2011;21:644–51.
[33] Samanta S, Manna U, Das G. White-light emission from simple AIE–ESIPT-excimer tripled single molecular system. New J Chem 2017;41:1064–72.
[34] Yu Liu MN, Wang Yue, Hou Zhaomin. π-Conjugated aromatic enynes as a single-emitting component for white electroluminescence. J Am Chem Soc 2006;128:5592–3.
[35] Wen Y, Liu H, Zhang S, Gao Y, Yan Y, Yang B. One-dimensional π–π stacking induces highly efficient pure organic room-temperature phosphorescence and ternary-emission single-molecule white light. J Mater Chem C 2019;7:12502–8.
[36] Tu D, Leong P, Guo S, Yan H, Lu C, Zhao Q. Highly emissive organic single-molecule white emitters by engineering o-carborane-based luminophores. Angew Chem Int Ed Engl 2017;56:11370–4.
[37] Wang J, Gu X, Ma H, Peng Q, Huang X, Zheng X, Sung SHP, Shan G, Lam JWY, Shuai Z, Tang BZ. A facile strategy for realizing room temperature phosphorescence and single molecule white light emission. Nat Commun 2018;9:2963.
[38] Williams EL, Haavisto K, Li J, Jabbour GE. Excimer-based white phosphorescent organic light-emitting diodes with nearly 100 % internal quantum efficiency. Adv Mater 2007;19:197–202.
[39] Xu S, Wang W, Li H, Zhang J, Chen R, Wang S, Zheng C, Xing G, Song C, Huang W. Design of highly efficient deep-blue organic afterglow through guest sensitization and matrices rigidification. Nat Commun 2020;11:4802.
[40] Tian Y, Yang J, Liu Z, Gao M, Li X, Che W, Fang M, Li Z. Multistage stimulus-responsive room temperature phosphorescence based on host–guest doping systems. Angew Chem Int Ed 2021;60:20259–63.
[41] Wang Y, Yang J, Fang M, Yu Y, Zou B, Wang L, Tian Y, Cheng J, Tang BZ, Li Z. Förster resonance energy transfer: an efficient way to develop stimulus-responsive room-temperature phosphorescence materials and their applications. Matter 2020;3:449–63.